Mullor Ruiz, I.; Vilariño-Feltrer, G.; Mnatsakanyan, H.; Vallés Lluch, A.; Monleón Pradas, M. (2021). Development and evaluation of hyaluronan nanocomposite conduits for neural tissue regeneration. Journal of Biomaterials Science Polymer Edition. 32(17):2227-2245. https://doi.org/10.1080/09205063.2021.1963930

Development and evaluation of hyaluronan nanocomposite conduits for neural tissue regeneration

Ismael Mullor Ruiz[1,2]. Guillermo Vilariño-Feltrer[1]. Hayk Mnatsakanyan[1]. Ana Vallés-Lluch[1,3]. Manuel Monleón Pradas[1,3]

1.- Centre for Biomaterials and Tissue Engineering. Universitat Politècnica de València. Camino de Vera s/n. 46022 València, Spain

2.- Department of Bioengineering. Imperial College London. Royal School of Mines. SW7 2AZ. London. United Kingdom

3.- Biomedical Research Networking Centre in Bioengineering, Biomaterials and Nanomedicine (CIBER-BBN). 46022 València, Spain

Abstract

Hyaluronan-based hydrogels are among the most promising neural tissue engineering materials because of their biocompatibility and the immunomodulation capabilities of their degradation byproducts. Despite these features, the problems related to their handling and mechanical properties have not yet been solved. In the present work it is proposed to address these drawbacks through the development of nanohybrid materials in which different nanometric phases (carbon nanotubes, mesoporous silica nanoparticles) are embedded in a crosslinked hyaluronan matrix. These nanohybrid matrices were next processed in the shape of cylindrical conduits aimed at promoting and improving neural stem cell differentiation and regeneration in neural tracts. These constructs could be of use specifically for peripheral nerve regeneration. Results of the study show that the inclusion of the different phases improved physico-chemical features of the gel such as its relative electrical permittivity, water intake and elastic modulus, giving hints on how the nanometric phase interacts with hyaluronan in the composite as well as for their potential in combined therapeutic approaches. Regarding the *in vitro* biological

behavior of the hybrid tubular scaffolds, an improved early cell adhesion and survival of Schwann cells in their lumen was found, as compared to conduits made of pure hyaluronan gels. Furthermore, the differentiation and survival of neural precursors was not compromised, despite alleged safety concerns.

Keywords: Hyaluronic Acid; Multiwalled carbon nanotubes; MWCNTs; Mesoporous Silica; Hydrogel; Neural conduit

1. Introduction

Axonal degeneration stands among the most hard-tackling medical issues worldwide due to several factors, such as the complex molecular underlying origin in some cases (e.g. Alzheimer[1,2] or Parkinson's disease[3,4], as well as in post-traumatic axonal diffuse damage[5]) or the zone where the damage takes place. For instance, damages in the central nervous system (CNS) rarely regenerate spontaneously because of the resulting reactive astrogliosis[6,7], while short-range injuries can be healed in the peripheral nervous system (PNS)[8-10]. All these constraints result in the current absence of a standardized effective treatment.

Tissue engineering for the nervous system[11] is a proposed approach to solve this problem, mainly focusing on the development of three-dimensional scaffolds that may assist and improve cell survival, growth and differentiation as well as achieve neural functional regeneration[12]. Hyaluronic acid (HA) is one of the most attractive materials with application in neural tissue engineering[13]. HA is a natural polymer consisting in repetitions of the N-acetyl-D-glucosamine and D-glucuronic acid dimer that can have a molecular weight that can oscillate between 10^3 and 10^4 Da[14]. HA is present in the extracellular matrix of many animal tissues like neural, connective and epithelial layers[14,15]. This polymer is characterized by many features that make scaffolds thereof very promising for biomedical applications: it is biocompatible[16-18], the greater molecular weight forms of HA have been shown to avoid the formation of scar tissue[19] and its low molecular weight byproducts of degradation have angiogenic and immunomodulative properties[20,-22]. Despite these virtues, HA is yet not entirely suitable for tissue engineering because of its handling difficulty and its considerable susceptibility to swelling and changing its volume in aqueous environments with different ionic strength[14,23-26]. For these reasons, different strategies have been postulated in the recent years in order to overcome its swelling instability. One of them is based on the use of chemical crosslinkers to obtain stable hylanes[27]. Despite the

success of the approach, the improvement is only partial, since the resulting hylanes still tend to lack good manageability and sometimes additional components are required.

In the present work, the proposed solution implies the use of nanoscale particles like multi-walled carbon nanotubes (MWCNTs) or mesoporous silica particles (UVM-7). The choice of these nanoscale materials relies on their exceptional reported mechanical properties[28,29], their potential to be used as carriers for controlled drug delivery[30,31], as well as previous works that have shown them to be interesting candidates[29,32,33].

The aim of the present study is to assess the adequacy of the use of these nanometric particles by evaluating if they improve the stability and mechanical properties of the hydrogels, and add novel functions. The potential removal of processing steps -like the addition of the crosslinkers in order to make the functional hylane- is also included under the scope of the present work. More precisely, the assessment will be done in a conduit-like structure that has previously proved to be suitable for the growth of neural support cells when made of crosslinked hylane[33-35]. In the present work, however, the biohybrid material will be environment of a co-culture of Schwann cells (SCs) with undifferentiated neurospheres (NSs), with the aim of triggering their differentiation to dopaminergic neurons. The tubular architecture of the scaffold, together with the induced cell differentiation within, would potentially be of interest for the repair of damage of peripheral nerve tissue.

2. Materials and methods

2.1. Hyaluronan hydrogels preparation

An aqueous solution of hyaluronan (HA) at 5% w/w was prepared by dissolving hyaluronan sodium salt obtained from *Streptococcus equi* (1.5-1.8 MDa, Sigma Aldrich) in a sodium hydroxide (NaOH, Sigma Aldrich) 0.2 M solution and gently stirring. Additional solutions with the nanometric components of the hybrids (MWCNTs and UVM-7) were prepared at 0.25% w/w and sonicated to disperse the nanometric components. The MWCNTs used for the elaboration of the nanocomposites (Sigma Aldrich) were synthesized by chemical vapor deposition and had estimated dimensions of 6-13 nm diameter and 2.5- 20 μm length. The mesoporous silica (UVM-7) on the other side, was kindly provided by Prof. Pedro Amorós, from the Institut de Ciència dels Materials at Universitat de València (Spain). These nanoparticles were obtained through a variation of the atranes synthesis route developed by Prof. Amorós group and previously reported in the literature[36-38]. These materials, accordingly, had an average size of about 200 nm, nanoparticle diameters of about 15−20 nm, and specific areas around 1,000 m^2/g, after sonication. The solutions were used at the stated concentration or diluted at 0.15% w/w, to obtain hydrogels with 3% and 5% (dry mass) of nanoloads, respectively named MWCNT.3 or UVM-7.3 and MWCNT.5 or UVM-7.5, depending on the nanoloads. Pure HA hydrogels were produced as controls. Both hyaluronan and nanometric-phase solutions were gently mixed with a magnetic stirrer for 24 h prior to the hydrogel preparation, followed by 30 min of thorough sonication. After these steps, divinyl sulfone (DVS; Sigma Aldrich) was added to the mixture in a proportion of 9 moles DVS for each 10 repetition units of the HA dimer. These solutions were injected in the corresponding molds immediately after DVS addition, according to their subsequent use.

For testing electrical conductivity of the gels as an indirect measurement of the dispersion of the nanometric components of the hydrogels, thin films (approximately 200 μm thick) were

prepared by gelling for 30 min a pre-adjusted volume of the HA solutions in 10 cm-diameter Petri dishes. Next, the films were vacuum-dried for 24 h to obtain non-porous substrates.

A second batch of hyaluronan solutions were injected in 10 cm-diameter Petri dishes, dried overnight at -20ºC and lyophilized for 24 h. The resulting scaffolds were withdrawn, hydrated for 24 h and die-cut to 5 mm-diameter discs of approximate height of 2 cm. To perform thermomechanical (TMA) and infrared spectroscopy (FTIR) analyses, as well as density and porosity tests, the discs were lyophilized again for 24 h.

The scaffolds intended for cell culture assays and those used in the morphological evaluation by electron microscopy (SEM) and swelling assays were injected in PFTE molds with 1.5 mm-sidesquared channels of 5 cm length. Prior to injection, a poly-ε-caprolactone (PCL) fiber of 400-450 µm diameter was held in the center of each channel through PTFE washers of 1.5 mm-side at both ends. After injection into these molds, the HA solution was gelled at room temperature for 10 min before freezing overnight at -20°C. Next, the assemblies were lyophilized for 24 h. Scaffolds were stored in dry conditions at -20°C. For their use in the tests, the scaffolds were extracted from the molds and the PCL fiber was removed by stretching it. Once the PCL fiber was removed, scaffolds were placed in water for 2 h and cut into 6 mm-length samples. Thus, it was possible to obtain crosslinked hyaluronan tubular scaffolds with a hollow channel inside, designed for neural regenerative purposes.

2.2. Stability in water of non-crosslinked HA nanohybrid scaffolds

To find out whether the nanoparticles enable interaction between linear HA chains to avoid it being dissolved in aqueous media without the need of a chemical crosslinker agent, two dilution tests were performed. First, a static test with non-crosslinked (without DVS) hydrogels immersed in a Petri dish with distilled water dish was performed for 24 h, taking high contrast photographs at different times. A similar test was performed in the same conditions but placing the Petri dishes on an orbital shaker for shorter periods of time (dynamic test). The images were later

processed with the ImageJ software (National Institutes of Health, USA) to measure the proportion of the area of each Petri dish occupied by the hydrogels and their detached fragments, considering the polygon with the minimum area encompassing all visible fragments.

2.4. Dielectric Spectroscopy properties of crosslinked HA nanohybrid scaffolds

Dielectric performance of the thin non-porous films was tested in order to obtain information about the nanometric phase dispersion and electric properties of the composites. This was achieved by applying an external alternating current (AC) electric field using a parallel-plates electrode capacitator (LCR Meter 4285A, Hewlett-Packard). The real and imaginary component of the impedance (resistance *R* and reactance *X*, respectively) was registered in the range from 75 to 1,000 kHz. The impedance, *Z = (R + Xi)*, is expressed as Equation (1) indicates:

$$Z = \frac{K}{(\sigma + \omega \cdot \varepsilon_0 \cdot \varepsilon_r \cdot i)} \quad (1)$$

where σ is the film electric conductivity, ω is the angular frequency, ε_0 is the electric vacuum permittivity, ε_r is the film electric permittivity and K is a measuring cell constant (film thickness/plates surface, in m^{-1}). σ and ε_r are characteristic parameters for each dielectric material and are highly descriptive with regard to dielectric behavior. Comparing them for each hydrogel composition, they can provide very useful information about the dispersion and percolation of the nanometric phase inside the hylane matrix in each nanohybrid. Thanks to a computer spreadsheet software (Mathcad, PTC) the *R* and *X* data fitting to Equation 1 was performed, through a non-linear Levenberg-Marquardt least square regression.

2.3. Morphological and physicochemical characterization

Scanning electron microscope (SEM) micrographs of the tubular scaffolds were taken in order to analyze in detail both the porosity and the pore interconnection. The lyophilized samples were first coated with gold.

In order to achieve supplementary information about chemical composition and functional groups, Fourier transformed infrared spectra (FTIR) were obtained with a Nicolet Nexus spectrometer (Thermo Scientific) from the analog flat scaffolds with different compositions.

To measure the density of the flat scaffolds, an AX205 precision balance (Mettler-Toledo) with a density determination module was used. By weighting the samples (N = 5 for each group) in their dry state and after immersion in n-octane, the density can be inferred as indicated in Equation (2):

$$\rho_{\alpha} = \frac{m_a}{m_p} \cdot \rho_0 \tag{2}$$

where ρ_0 = 0.703 g/ml is the density of n-octane (Sigma-Aldrich), m_a is the mass of the dry scaffold and m_p is the mass of the scaffold immersed in n-octane. To measure m_p, the scaffolds were previously placed in n-octane and the solvent forced to fill their pores by applying vacuum with a pump for 5 min.

Water uptake of the tubular scaffolds from the dry state was measured at equilibrium under two different conditions: in a chamber with relative humidity of 97% and immersing the samples in phosphate buffer saline (Dulbecco's Phosphate Buffered Saline, Merck), both at 37°C. The scaffolds' mass was then measured over time with an AX205 precision balance (Mettler-Toledo), after gently removing superficial non-absorbed water. The water content for each time point (WC) was calculated according to Equation (3):

$$WC = \frac{m_i - m_0}{m_0} \tag{3}$$

where m_i corresponds to the mass of hydrogel at time *i*, and m_0 is the dried hydrogel (xerogel) mass. To determine the equilibrium water content (EWC), the average mass data of each sample at the steady state was considered as the equilibrium mass, m_∞, and substituted for m_i in equation 3. Number of replicates for each type of material was N = 4.

Thermomechanical analyses (TMA) of flat scaffolds (N = 5) were carried out with a dilatometer (Exstar SS6000, Seiko Instruments) in the compression mode, from 50 to 1,500 mN at 100 mN/min. Measurements were performed at 37ºC with the samples immersed in DPBS, in order to simulate physiological conditions. The elastic moduli were calculated as the slope of the pseudo-linear sectors of the stress-strain plot, before and after the plateau region. The "low strain" (10% initial strain) and "high strain" moduli (last 5% strain) were named as E_1 and E_2, respectively.

2.4. Biological assays

As for the biological response of the tubular scaffolds, only those with 5% w/w of nanoparticles (referred to the dry weight of the scaffold, *i.e.*, 0.25% w/w in the initial suspension) and the controls without nanoparticles were used, as it was hypothesized that a higher proportion may have an acuter, more visible effect.

Rat Schwann cells (SCs) from a commercial line (Innoprot) were expanded to passage 5 with Schwann Cell Medium (SCM, Innoprot) and seeded within the lumen of the hydrogel channeled conduits at $5 \cdot 10^4$ cells per scaffold by means of a 5 µl Hamilton syringe.

After 2, 6 and 10 days of culture with SCM at 37ºC and 5% CO_2, an MTS viability assay kit (CellTiter 96 Aqueous One Solution Cell Proliferation Assay, Promega) was used to determine cell density by colorimetry with a multilabel plate reader (Victor^3 1420, Perkin Elmer) at 490 nm.

In order to assess the survival and differentiation of neurons for our proposed tissue regeneration application, the SCs were co-cultured with neurospheres (NSs) for the rest of the studies. NSs were extracted from the subventricular zone of mice and transfected with red fluorescent protein (RFP) in passage 4. These cells were kindly provided by Prof. José Manuel García Verdugo, from the Department of Cell Biology, at Universitat de València, Spain. The NSs were first pre-cultured for 4 days in a 12-well plate pre-treated during 3 h with fibronectin to

expand them and make them express nestin (Human/Mouse Dopaminergic Neuron Differentiation Kit, R&D Systems). After that, NSs were seeded at $1.2 \cdot 10^4$ NSs/disc in 5 mm-height and 6 mm-diameter discs made of 1% agar suitable for cell cultures (Sigma Aldrich) with a 1.5 x 1.5 x 3 mm slot each. Conduits with SCs seeded inside for 10 days (see the procedure above) were set vertically inside the agar discs slots to fasten the NSs at their bottom end. The co-seeded cells were incubated for up to 9 days.

To supplement data on cell viability and to settle whether the materials were able to support the survival and differentiation of neurons, a Western blot with dopaminergic lineage markers was carried out. The dopaminergic lineage markers used to address whether a dopaminergic phenotype was developed and kept were the phosphorylated form of Tirosin Hydroxylase (TH) and Beta III Tubulin. TH was chosen because it has a fundamental role in the synthesis of catecolamin, dopamine, noradrenalin and adrenalin and when phosphorylated becomes much more active, which is required by the dopaminergic phenotype exclusive of neurons. Beta III Tubulin, on the other hand, is a microtubule protein that is expressed exclusively on neural linages. Moreover, a finer quantification of the fraction of neurospheres differentiated into dopaminergic neurons, with respect to the total number of neurons, would not require a GADPH loading control since both proteins are being measured in the same Western Blot membrane, so it could be obtained by measuring the ratio signal between pTH and Beta III tubulin. The protein extraction was run as specified by the extraction reagent N-PER protocol (Thermo Scientific), incubating the reagent for 5 min on ice with 3 seeded scaffolds of each type after 5 and 9 days of co-culture. Thereafter, the cell lysate was collected in an Eppendorf tube and centrifuged at 10,000 g for 10 min to next analyze the supernatant from the tube. Protein separation was carried out on polyacrylamide gels of SDS-PAGE at 10%, using the BioRad kit for Western Blotting (MiniProtean Tetra Cell) and filling the tray with twice running buffer. Along with the extract, previously mixed and homogenized with 10 µl of loading buffer (BioRad), 10 µl of marker protein bands (PageRuler Prestained Protein Ladder, Piercenet), were incorporated.

The proteins were separated with running buffer (BioRad) at 50 V per gel for 1.5 h until the 170 kDa band entered the resolving gel fraction, and before the 28 kDa band came out of it. Once separated, the proteins were transferred to PVDF membranes positively charged (GE Healthcare). They were activated with methanol for 30 s, rinsed with deionized water for 5 min and placed in a transfer buffer (BioRad). Membrane transfer was performed at constant 20 V for 45 min. After that, the membranes were incubated with blocking buffer (DPBS + Tween-20 0.1% w/v. Sigma Aldrich) + powder milk 5% w/v (Sigma-Aldrich) for 30 min in a rocker shaker. After blocking the membrane, it was incubated with the primary antibody for each protein (rabbit anti-tyrosine hydroxylase and mouse anti-beta-III tubulin -all from Abcam-, diluted at 1:1,000 in blocking buffer + 2% powder milk). Primary antibodies were incubated overnight at 4°C and shaken 1 h at room temperature. After that, the membranes were rinsed twice with PBS and the secondary antibody incubation was performed for 2 h under stirring at room temperature with goat anti-rabbit and goat anti-mouse joined to HRP (GE Healthcare) diluted at 1:20,000 in blocking buffer + 2% powder milk. Three rinses with blocking buffer and six PBS washes of 10 min each under stirring were performed next. After washing, the chemiluminescent substrate ECL Plus (Thermo Fisher) was applied to the membranes for 5 min and subsequently they were put in the cassette with the developer film (30 s exposure). As a comparative control, a co-culture was performed on a plate well without the scaffold nor the agar.

A fluorescence immunocytochemistry staining was performed to evaluate the morphology of the cells grown inside the tubular scaffolds' lumen. After 5 and 9 days of culture, the different co-cultured scaffolds were washed twice with PBS at 37°C, fixed with paraformaldehyde (PFA) 4% in PBS 15 min, washed three times with PBS at 4°C, 5 min each, and incubated 30 min in blocking buffer + 1% BSA. The samples were incubated at 4ºC with rabbit anti-tyrosine hydroxylase (TH, 1:1,000 in blocking buffer, Abcam) or mouse anti-beta III tubulin (βIII-Tub, 1:500 in blocking buffer, Abcam), both overnight. Then, the cultured scaffolds were rinsed two times in PBS prior to incubation with secondary antibodies goat anti-rabbit AlexaFluor 488 or

goat anti-mouse AlexaFluor 488, depending on the protein targeted, both 1:200 in blocking buffer (Abcam) at room temperature. Lastly, they were stained 10 min with DAPI (1:5,000 in blocking buffer, Sigma-Aldrich) and washed with PBS three times, after which the scaffolds were cut longitudinally and mounted with a glass coverslip to observe them all along the lumen with a fluorescence microscope (Nikon Eclipse 80i). Double immunocytochemistry staining was not conducted to reveal the presence of both proteins simultaneously on suspicion that, after co-culture, NSs could still be expressing RFP, which helped identification and growth monitoring at earlier stages.

2.5. Statistical analysis

To determine significant differences between groups in experiments with a sufficient sample size, an ANOVA study was conducted. Alongside, post-hoc mean comparison tests between groups were performed when possible with the statistical analysis software Statgraphics Centurion XVI (StatPoint Technologies). When the variance determined for all groups was similar (cell viability assays), the Fisher's multiple range least significant differences (LSD) criterion was selected. Scheffé method was preferred otherwise when there were significant differences between the variances of different groups.

3. Results and discussion

3.1. Stability of non-crosslinked nanohybrids

Figure 1 shows the relative area occupied by the scaffold fragments (A) expressed as a percentage of the total area in static (B) and dynamic conditions (C). As can be seen, pure HA samples and those loaded with UVM-7 eventually get completely scattered throughout the whole area of the Petri dish. When MWCNT3% and 5% samples were left to disperse undisturbed, the scaffolds degraded partially to cover 50% and 30% of the available surface in 4h, respectively, and appeared to remain constant after this point. In the dynamic test, however, the differences between MWCNT3% and 5% samples were not suchlike, and their fragments dispersed over the 60% of the Petri dish area after only 60 min. These observations indicate that the scaffolds containing dispersed MWCNTs present an enhanced water stability in comparison to those with UVM-7 or the controls, yet it is not enough to ensure the stability of the conduit without crosslinker addition, thus making the step of the cross-linker addition a necessary one in the fabrication of microconduits.

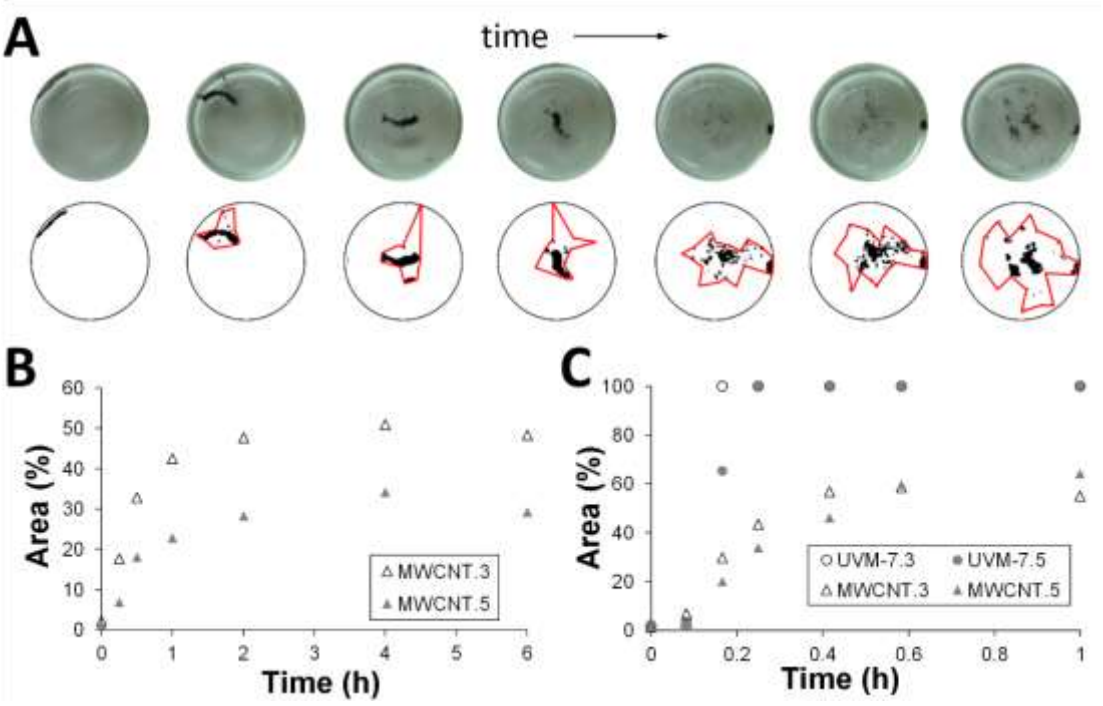

Figure 1. (A) Time-lapse evolution of the dissociation of the HA-MWCNTs 5% scaffold in orbital shaking used as an illustrative example on how the degradation and the area associated with it in the Petri dish were taken and calculated. (B) Quantified degradation (area) of the scaffolds in static conditions. (C) Quantified degradation of the scaffolds under active shaking.

3.2. Dispersion of the nanometric phase in the hydrogels

Figure 2 shows the morphology of the nanohybrid conduits under electron microscopy. While the nanoload features seen in Figure 2A and 2B were too small to identify their dispersion throughout the nanohybrids (Figure 2C, 2D), the overall porosity of these seemed to remain unaffected, as compared to the HA conduits in Figure 2E. Still, the average pore size of the nanoconduits was apparently reduced when MWCNTs were present, along with the shape of the formed lamella, that seemed slightly different.

More images were taken from sections corresponding to the inner wall matrix of the conduit, as well as the external walls that were in contact with the PFTE during the casting and freeze-drying of the nanohybrid conduits (data not shown). When comparing them, no significant differences in terms of morphology were observed between the different composites, despite all surfaces in contact with the PTFE mold appeared more flattened.

Figure 3A shows the electric AC conductivity of dry HA-based films as a function of the frequency of the current of the electrodes. On this image all the nanocomposites seem to have a similar conductivity behavior (with slightly lower values for HA-MWCNT hybrids) in the range matching the reported values for hyaluronan alone[39], despite the presence of the nanometric phase embedded within the composite.

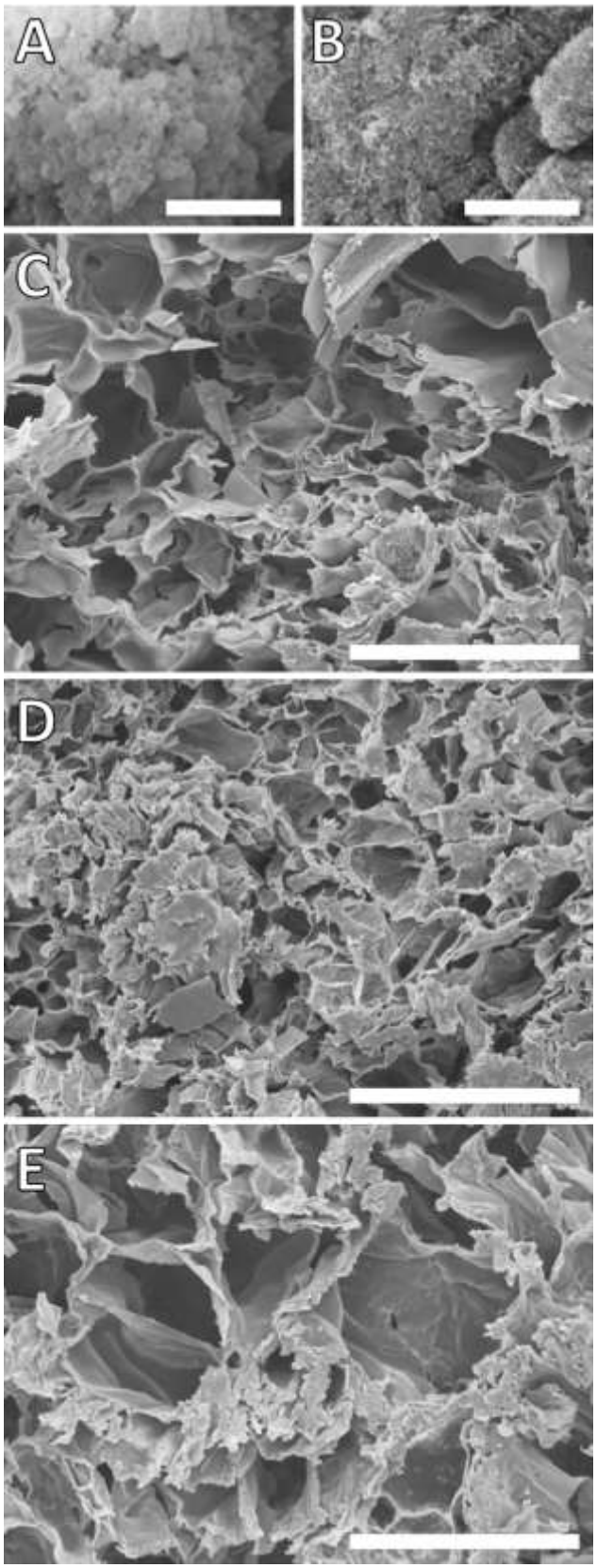
A
B
C
D
E

Figure 2. SEM images of the (A) UVM-7 or (B) MWCNT nanoloads. (C-E) SEM images of the internal matrix of (C) UVM-7.5 and (D) MWCNT.5 nanohybrids and (E) HA scaffolds. Scale bar = (A, B) 5 μm and (C-E) 100 μm.

The difference between materials is revealed when observing the relative permittivity, which is around 2 in all cases except in the composite with a 5% dry weight of MWCNTs, which begins with a relative permittivity of 15 but drops as the frequency increases, indicating that the dielectric polarization mechanisms within the composite are becoming deactivated, which is expected to happen in high frequencies. When comparing the values of the dielectric properties between all the materials, it can be observed that the conductivities of all of them share orders of magnitude. This feature does not match with other data on the bibliography in which the addition of carbon nanotubes resulted in high augmentations of the electric conductivity of the material[40], which indicates that the MWCNTs are not dispersed continuously throughout the composite.

The hypothesis of the discontinuity of the dispersion of the nanometric phase in the hyaluronan matrix gets more support in the literature. Indeed, a nematic liquid crystal behavior of the SWCNTs in hyaluronan acid solutions has been reported and attributed to Van der Waals forces[41], thus breaking the homogeneity of the dispersion. Although this behavior was described for SWCNTs, the results can be transposed to our present case since the forces driving the process are ubiquitous Van Der Waals forces, which are also present in both nanometric phases. This same reference also determined that homogeneous dispersion of these carbon nanotubes was poor in highly viscous solutions, for which gave an example of a 2% w HA solution –a concentration less than half that used in these nanocomposites. It must be noted that in all cases the conductivity of the materials was in the range of the semiconductor ones[42] and in the case of the materials with the 5% dry weight of MWCNTs it can be observed that the relative

permittivity at the lowest frequencies was comparable to that of some intrinsic semiconductors such as silicon or germanium[42], thus opening possibilities regarding combined therapeutical applications of the material within tissue engineering as a neural interface material. It must be said that in the case of UVM-7 particles, previous work by Vallés-Lluch *et al.*[29] showed that it was possible to achieve a continuous silica phase throughout the hylane matrix. However, the UVM-7 particles were in that work previously pre-dispersed in a NaOH solution and sonicated instead of the conventional stirring followed here, thus accounting for the differences in dispersion observed after the two procedures.

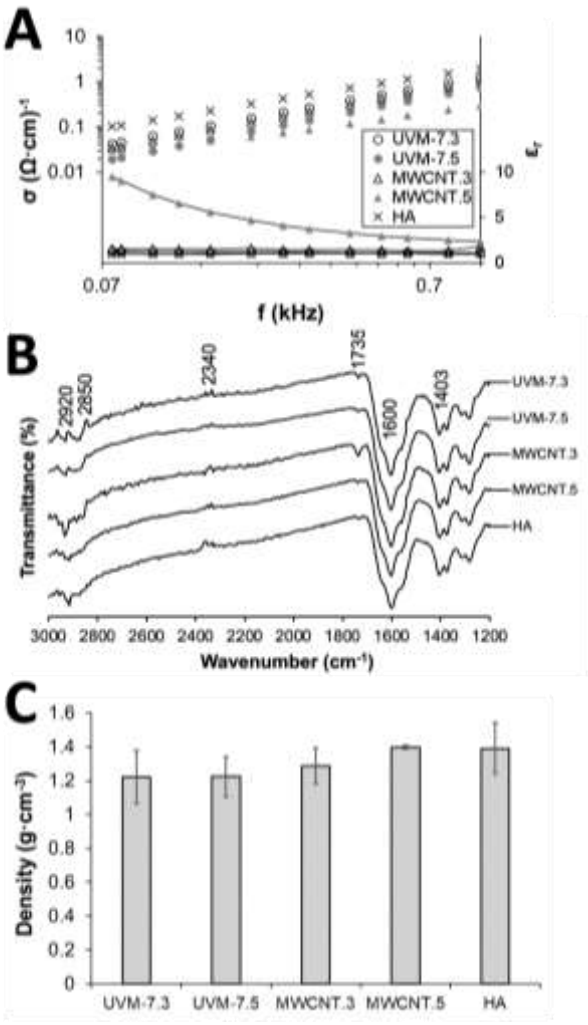

Figure 3. (A) Electric conductivity (left) and dielectric permittivity (right) of the nanohybrids as a function of the frequency of the alternate electric current. FTIR spectra (B) and density (C) of

the freeze-dried HA nanocomposites. Density data are presented as mean ± standard deviation.

Figure 3B shows the FTIR spectra for the dry flat scaffolds with different nanoparticle compositions. Only the wavenumber ranges where differences were detected between spectra or where the main characteristic peaks of HA laid are displayed. Slight differences among each spectrum due to the different nanometric phases embedded on the hyaluronan matrix at 2,340, 2,850 and 2,920 cm^{-1} can be observed. A slight signal peak appears at 1,735 cm^{-1}, corresponding to a C=N vibration mode from the amino bonds of the hylane. However, in the samples with nanometric phase it can be observed that the lower concentration (3%) broadens and makes this peak more noticeable, whereas the higher concentration (5%) totally mask its presence. At 2,340 cm^{-1} the displaced stretching node of Si-OH bonds of UVM-7[43] nanoparticles appears, while the other two peaks at 2,850 and 2,920 cm^{-1} correspond to a shifted stretching of the Si-OH bond. The effect of the intensity reduction through the IR radiation shielding is obvious on them. Two of the typical peaks of hyaluronic acid (1,403 and 1,600 cm^{-1}, those corresponding to C-O and asymmetric C=O bonds stretching[44]) can be clearly distinguished for all tested films, with an alike shape in all cases. Although all spectra presented a small shift, the effect is equivalent for all samples. In summary, little differences among the FTIR spectra are observed and can be attributed in each case to characteristic chemical bonds present in the nanoparticle, such as the Si-H bond at 2,350 cm^{-1} of the UVM-7-loaded hydrogels or the peaks corresponding to the stretch of the Si-OH bond around 3,000 cm^{-1}. This observation suggests that during the material processing the nanometric phase does not react nor suffers any change on its composition. It could also be argued, given that MWCNTs signals are in zones where there is overlapping with signals from the hyaluronan, that signal-quenching seen on the MWCNTs composites when compared to the control is a hint of their presence, since they are masking slightly those signals.

Figure 3C displays the density of the dry nanocomposites and the control, calculated using Equation 2. No significant differences were observed in this parameter, despite the presence of the embedded nanoparticles. The comparable densities could be taken in principle as a first favorable yet insufficient evidence of the composites' compatibility, since density and bulk response of implants are related with cell adhesion and survival[44] in living tissues, and the control reference has already proved to be suitable to such purpose in similar contexts[35-37]. Immersion in n-octane also allowed us to roughly estimate the porosity of the dry materials (> 97% in all cases).

3.3. Water intake

Figure 4 displays the equilibrium water intake (EWC, in equation 3) (A) in a vapor saturated atmosphere and (B) in DPBS, attained after 192 h and 2 h, respectively. Differences beyond these time-points were negligible and for this reason the span to reach the equilibrium state was set there. The scaffolds with carbon nanotubes or the mesoporous silica nanoparticles absorbed more water that the control (Figure 4A). Conversely, the controls reach the highest water uptake in DPBS (Figure 4B). The response of the HA-based materials to swelling and the modulation of their mechanical properties by CNTs and nanosilica was investigated. The presence of nanoparticles increased the water uptake from a humid vapor phase, whereas in liquid DPBS the hydrogels without particles were those that retained more water. This feature can be explained in terms of the different mechanisms that rule water intake in each case: in the saturated atmosphere sorption in available places of hyaluronan is the main mechanism and in this case the presence of the nanometric phase and its discontinuities acts opening the hyaluronan network and letting more sorption sites become available, being this effect more remarkable the smaller the nanoparticle, as can be seen with MWCNTs versus UVM-7 (the former are smaller). When swollen in DPBS, all sorption sites are rapidly occupied and in the presence of more water the hyaluronan network gets forced to open to allow the intake of more water in

order to reach thermodynamic equilibrium[45,46], the presence of the nanoparticles being an obstacle to tackle rather than an aid for the swelling. This property, in biological contexts, can help to a much more controlled water intake than that of hyaluronan on its own, resulting in a better performance overall because the material is less deformed upon the environmental water intake. We must note that the EWC of the HA-MWCNTs nanohybrids is coherent in both cases with the values obtained by Arnal-Pastor *et al.*[32] for their freeze-dried hydrogels. However, this is not the case with the HA-UVM-7 nanohybrids when compared with the previous experimental results of Vallés-Lluch *et al.*[29], but again, there are several methodological differences between the present and the cited work. More particularly, the hydrogels here used are freeze-dried whereas those nanohybrids were dried at room temperature first and then 24 h into vacuum and pre-washed before experiments.

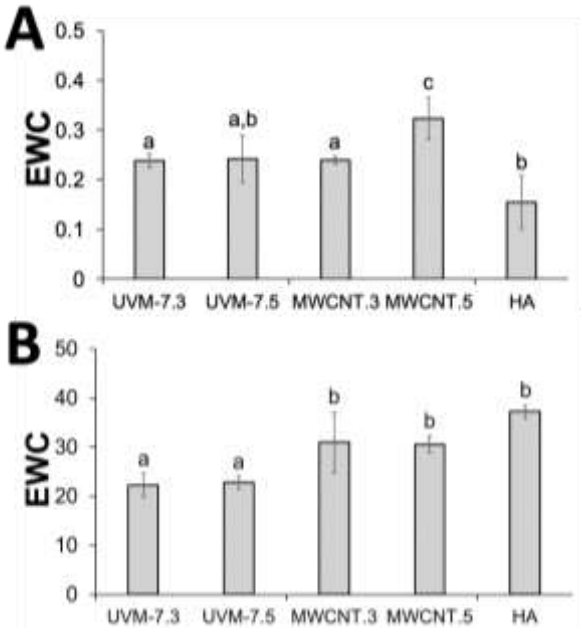

Figure 4. Equilibrium Water Content (A) at 97% relative humidity and (B) following immersion in DPBS of the nanohybrids. Data are presented as mean ± standard deviation. Homogeneous groups are expressed with the same letter.

3.4. Mechanical properties

Figure 5A displays the typical stress-unitary strain behavior of a crosslinked HA hydrogel, as an example, and how the E_1 and E_2 moduli were determined through the slope of the pseudo-linear regions. Figures 5B and C show the calculated compressive elastic moduli of the flat scaffolds with different nanoparticles in the low compression and high compression (near to the collapse point) zones, respectively. In the low compression zone, the behaviour observed corresponds to that of the porous material and the progressive collapse of the pores. The second linear zone can be attributed to the bulk material. The average values of E_2 (450-600 kPa) were at least an order of magnitude higher than those of E_1 (17-67 kPa). Despite the variability of the samples, it is clear that the presence of a nanometric phase in the HA scaffolds changes the profile of the Young moduli when incorporated at a 5% dry weight. On the other hand, no remarkable differences were observed on the moduli when approaching the collapse point. It is arguable whether at low compressions the presence of the nanometric phase increases the elastic modulus, this improvement being dependent of its concentration. This situation is apparently explained by the dimensions, since the MWCNTs or the UVM-7 are small and compact enough in the hyaluronan matrix to support stresses when compressed, this effect being greater the smaller the particle size nanometric phase is –as in the case of the MWCNTs. It must be remarked also that the Young moduli of the UVM-7 gels in the second regime is much lower than reported on previous preparations containing this silica-based materal[29]. More precisely, for the materials with 5% dry weight of UVM-7, the Young modulus varies from 2 MPa reported in previous works to 0.5 MPa observed here. Again, this variation may be due to the different preparatuion of the materials in terms of the dispersion of the UVM-7 in the hylane matrix as well as the freeze-drying process, thus explaining the variation. In any case, this higher Young moduli in the materials with the nanometric phase might result in a greater biological viability of seeded cells within it. This is due to the fact that a higher Young modulus implies a greater stiffness that both

can affect cell adhesion[44] as well as offer the cells a greater protection from external mechanical stresses[47].

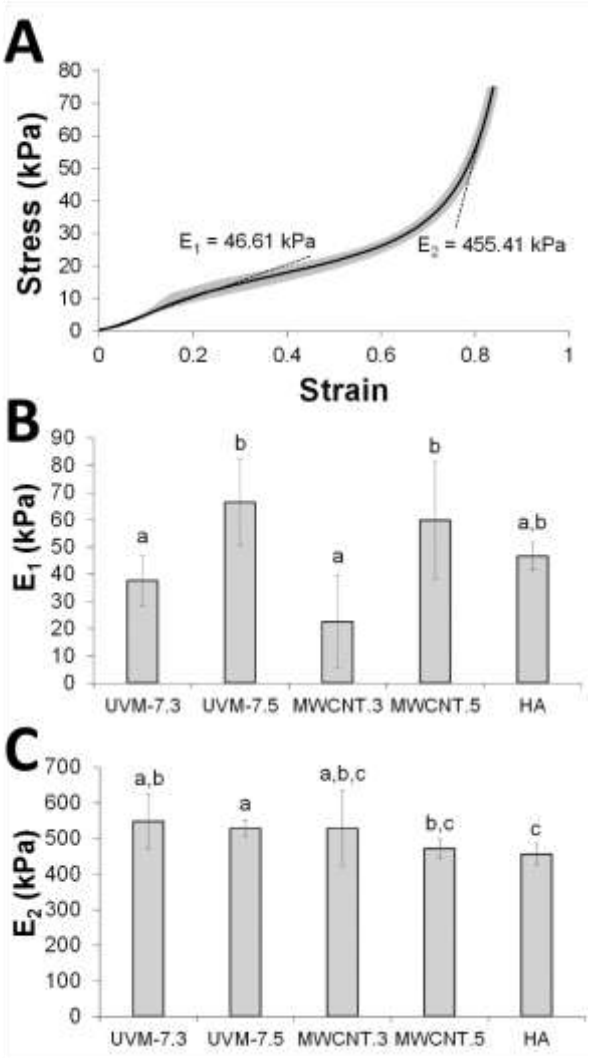

Figure 5. (A) Average behaviour of a swollen hydrogel material in a TMA measurement and procedure for low-strain and high-strain Young moduli evaluation over the pseudo-linear regimes. The gray shade represents ± standard deviation for each unitary strain datum. Low-strain (B) and high-strain (C) Young moduli of the nanohybrids. Homogeneous groups are expressed with the same letter.

3.5. Biological development

Our designed conduit-shaped nanohybrids are designed to act as implants to regenerate the nigrostriatal tract in animal models of Parkinson's disease. For these implants to be functional, we intend to promote the differentiation of neural precursors into dopaminergic neurons inside the inner channel of the conduit and restore the connections between the damaged peripheral nerves. Hence, the tests of biological development are aimed to assess in vitro how the differentiation steps into dopaminergic cells occur in the nanohybrids. However, while the nanohybrid conduits were initially designed for regeneration of damages derived of Parkinson's disease, they could also be applied for the regeneration of damages of peripheral nerves.

Figure 6A shows the absorbance measured after the treatment of the cell cultures inside the channeled conduits using the colorimetric assay, as previously described. The absorbance, expressed in arbitrary units, is linearly dependent of the cell metabolism and, therefore, can be directly related to the number of functional SCs present inside the conduits after 2, 6 and 10 days of culture. Absorbance mean values were significantly higher for the nanohybrids after 2 and 6 days of cell culture, as compared with the control. At day 10, the viability assay detected a similar amount of general metabolic activity or all samples, though. It seems, thus, that the presence of the nanometric phase within the hydrogel is not only not detrimental for the glial cells cultured but favours cell growth in the early stages of the essay as per the greater values in the MTS assay. Potential explanations for this behaviour could be associated with the greater elastic modulus measured derived from the lower swelling that composites present compared to the hylane-only hydrogel, discussed in Section 3.4.

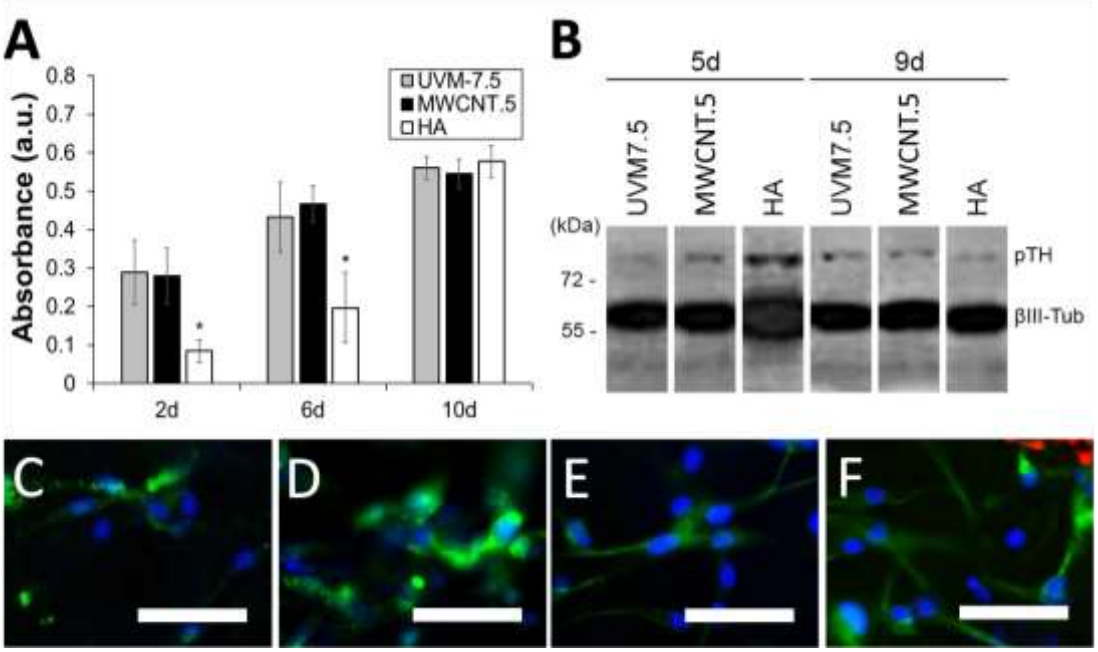

Figure 6. (A) Absorbance results for the MTS assay performed in Schwann cells seeded in the lumen of the nanohybrid conduits and cultured for 2, 6 and 10 days. An asterisk represents a statistically significant difference with the other groups. (B) Western Blot for phosphorylated tyrosine hydroxylase (pTH) and βIII-tubulin (βIII-Tub) of protein extracts from different nanohybrids cultured 10 days with SCs and additional 5 or 9 days with NSs. (C-F) Fluorescence microscopy images of SCs + NSs co-cultured for 5 (C, E) or 9 days (D, F) on UVM-7.5 nanohybrids and immunostained for TH (C, D) or βIII-Tub (E, F). Blue staining corresponds to the DAPI staining of the nuclei whereas green signal corresponds with the antibody for the immunostaining on each case. Scale bar = 50 µm.

Figure 6B shows the results of the Western Blot (WB) analysis performed on cell cultures in which a pre-differentiation of rat neurospheres was induced to neuron-type cells. The presence of markers for dopaminergic differentiation (phosphorylated tyrosine hydroxylase, βIII-tubulin)[48] were assessed in this assay. The Western blot shows that the differentiation markers[49] to dopaminergic neurons are properly expressed. The cells morphology, on the other hand, is that expected for neuronal cells, which overall shows that the first steps on the biomaterial evaluation are favorable. However, a further evaluation of the cell health must be done. For this,

we performed two immunofluorescence assays for the chosen differentiation markers in order to understand how they were distributed throughout the cells, as well as their morphology. Figure 6C displays the immunofluorescence images for DAPI staining (the nucleus) in blue, beta–III-tubulin in green and the formed axons and tyrosin hydroxylase in red. As can be observed, and in agreement with the Western blot results, all differentiation markers are expressed, and after 5 and 9 days the cell morphology has evolved from that of a neurosphere to that typical of a dopaminergic neuron, thus giving a further confirmation of a successful viable differentiation.

4. Conclusions

In this work, the addition of carbon nanotubes and silica nanoparticles to hyaluronan, particularly shaped as tubular nanohybrid scaffolds, was studied in order to explore their suitability for the regeneration of tubular neural structures. The effect of the different properties of the nanoparticles embedded (such as size and morphology) was related with improvements of the hydrogel properties. Generally, it was observed that the addition of the UVM-7 and the MWCNTs provoked a decrease of the swelling capability of the hydrogel and in turn, increased its Young modulus. We postulate, based in this finding, that the addition of the nanometric phase to the hyaluronan conduits provides a new tunable design variable. Moreover, changing variants such the dispersion mode, or the chemical properties of the nanometric phase is a potential solution to some of the posed difficulties for the usage of hyaluronan in tissue engineering, such as its poor dimensional stability and mechanical properties. The biological characterization shed some light on the possible controversy surrounding the nanoparticles' safety issues. The presence of such nanoparticles in the hyaluronan matrix was not detrimental for cell viability at the culture times under study and could potentially improve early cell survival, what is critical in the context of the tissue engineering applications of the material for ensuring the therapeutic success. It must also be noted that the hinted electric properties of the composites with 5% dry weight of MWCNTs, along with their biocompatibility, opens up applications of these materials other than hydrogels for regenerative purposes, such as in prosthetic neurotechnological devices for electric stimulation.

Acknowledgements

The authors acknowledge funding through the MAT2011-28791-C03-02,03 project from the Spanish Ministerio de Economía y Competitividad. The authors thank deeply the advice of C. Martínez Ramos, Ph.D. on the cell culture tasks, Prof. J. M. Meseguer Dueñas on the dielectric

impedance spectroscopy, and S. Ivaschenko with FTIR spectroscopy. Lastly, Prof. P. Amorós from Institut de Ciència de Materials of Universitat de València (ICMUV) and Prof. J. M. Verdugo are thanked for providing the mesoporous silica nanoparticles and the rat neurospheres, respectively. The Electronic Microscopy Service of the Universitat Politècnica de València is acknowledged their help and dedication.

Data availability

The raw/processed data required to reproduce these findings cannot be shared at this time as the data also forms part of an ongoing study.

References

[1] A. Mudher, S. Lovestone, Alzeheimer's desease-do tauists and Baptists finally shake hands?, Trends Neurosci. 25 (2002) 22-26.

[2] P.N. Lacor, M.C. Buniel, P.W. Furlow, A. Sanz Clemente, P.T. Velasco, M. Wood, K.L. Viola, W.L. Klein, AB oligomer-induced aberrations in synapse composition, shape, and density provide a molecular basis forloss of connectivity in Alzheimer's disease, J. Neurosci. 27(4) (2007) 796 –807.

[3] A. Schapira, Neurobiology and treatment of Parkinson's disease, Trends Pharmacol. Sci. 30 (2009) 41–47.

[4] N. Singh, V. Pillay, Y. Choonara, Advances in the treatment of Parkinson's disease, Prog. Neurobiol. 81 (2007) 29–44.

[5] V.E. Johnson, W. Stewart, D.H. Smith, Axonal pathology in traumatic brain injury, Exp. Neurol. 246 (2013) 35–43.

[6] M.V. Sofroniew, Molecular dissection of reactive astrogliosis and glial scar formation, Trends Neurosci. 32(12) (2009) 638-647.

[7] J. Silver, J.H. Miller, Regeneration beyond the glial scar, Nat. Rev. Neurosci. 5(2) (2004) 146-156.

[8] G. Stoll, S. Jander, R.R. Myers, Degeneration and regeneration of the peripheral nervous system: from Augustus Waller's observations to neuroinflammation, J. Peripher. Nerv. Syst. 7(1) (2002) 13-27.

[9] F.J. Liuzzi, B. Tedeschi, Peripheral nerve regeneration, Neurosurg. Clin. N. Am. 2(1) (1991) 31–42.

[10] N. Dubey, P.C. Letourneau, R.T. Tranquillo, Guided neurite elongation and Schwann cell invasion into magnetically aligned collagen in simulated peripheral nerve regeneration, Exp. Neurol. 158 (1999) 338–350.

[11] R. Langer, J.P. Vacanti, Tissue engineering, Science 260(5110) (1998) 920-926.

[12] J.S. Belkas, M.S. Shoichet, R. Midha, Peripheral nerve regeneration through guidance tubes, Neurol. Res. 26(2) (2004) 151-160.

[13] X. Wang, J. He, Y. Wang, F.Z. Cui, Hyaluronic acid-based scaffold for central neural tissue engineering, Interface Focus 2 (2012) 278–291.

[14] L. Lapcík Jr., L. Lapcík, S. De Smedt, J. Demeester, P. Chabrecek, Hyaluronan: Preparation, Structure, Properties, and Applications, Chem. Rev. 98(8) (1998) 2663-2684.

[15] R.U. Margolis, R.K. Margolis, L.B. Chang, C. Preti, Glycosaminoglycans of brain during development, Biochemistry 24(1) (1975) 85-88.

[16] J. Lam, N.F. Truong, T. Segura, Design of cell–matrix interactions in hyaluronic acid hydrogel scaffolds. Acta Biomater. 10(4) (2014) 1571-1580.

[17] Y. Lei, S. Gogjini, J. Lam, T. Segura, The spreading, migration and proliferation of mouse mesenchymal stem cells cultured inside hyaluronic acid hydrogels, Biomaterials 32(1) (2011) 39–47.

[18] T. Wang, M. Spector, Development of hyaluronic acid-based scaffolds for brain tissue engineering. Acta Biomater. 5 (2009) 2371–2384.

[19] Z.Z. Khaing, B.D. Milman, J.E. Vanscoy, S.K. Seidlits, J.G. Raymond, C.E. Schmidt, High molecular weight hyaluronic acid limits astrocyte activation and scar formation after spinal cord injury, J. Neur. Eng. 8(4) (2011) 046033.

[20] S. Matou-Nasri, F. Gaffney, S. Kumar, M. Slevin, Oligosaccharides of hyaluronan induce angiogenesis through distinct CD44 and RHAMM-mediated signalling pathways involving Cdc2 and gammaadducin, Int. J. Oncol. 35 (2009) 761-773.

[21] B.M. Tesar, D. Jiang, J. Liang, S.M. Palmer, P.W. Noble, D.R. Goldstein, The role of hyaluronan degradation products as innate alloimmune agonists, Am. J. Transplant. 6(11) (2006) 2622-2635.

[22] S. Yung, T.M. Chan, Pathophysiology of the peritoneal membrane during peritoneal dialysis: the role of hyaluronan, Biomed. Res. Int. (2011) 180594.

[23] B.V. Slaughter, S.S. Khurshid, O.Z. Fisher, A. Khademhosseini, N.A. Peppas, Hydrogels in regenerative medicine. Adv. Mater. 21(32-33) (2009) 3307-3329.

[24] O. Jeon, S.J. Song, M.H. Park, S.H. Lee, S.K. Hahn, S. Kim, B.S. Kim, Mechanical properties and degradation behaviors of hyaluronic acid hydrogels cross-linked at various cross-linking densities, Carbohydr. Polym. 70 (2007) 251–257.

[25] P.C. Georges, W.J. Miller, D.F. Meaney, E.S. Sawyer, P.A. Janmey, Matrices with compliance comparable to that of brain tissue select neuronal over glial growth in mixed cortical cultures, Biophys. J. 90 (2006) 3012–3018.

[26] S.K. Seidlits, Z.Z. Khaing, R.R. Petersen, J.D. Nickels, J.E. Vanscoy, J.B. Shear, C.E. Schimidt, The effects of hyaluronic acid hydrogels with tunable mechanical properties on neural progenitor cell differentiation, Biomaterials 31(14) (2010) 3930-3940.

[27] C. Schanté, G. Zuber, C. Herlin, T. Vandamme, Chemical modifications of hyaluronic acid for the synthesis of derivatives for a broad range of biomedical applications, Carbohydr. Polym. 85 (2011) 469–489.

[28] M.F. Yu, O. Lourie, M.J. Dyer, K. Moloni, T.F. Kelly, R.S. Ruoff, Strength and breaking mechanism of multiwalled carbon nanotubes under tensile load, Science 287(5453) (2000) 637-640.

[29] A. Vallés-Lluch, S. Poveda-Reyes, P. Amoros, D. Beltrán, M. Monleón Pradas, Hyaluronic Acid–Silica Nanohybrid Gels, Biomacromol. 14(12) (2013) 4217-4225.

[30] A. Bianco, K. Kostarelos, M. Prato, Applications of carbon nanotubes in drug delivery, Curr. Opin. Chem. Biol. 9 (2005) 674–679.

[31] J. Lu, M. Liong, J.I. Zink, F. Tamanoi, Mesoporous silica nanoparticles as a delivery system for hydrophobic anticancer drugs, Small 3(8) (2007) 1341-1346.

[32] M. Arnal-Pastor, C. Tallà Ferrer, M. Herrero Herrero, A. Martinez-Gomez Aldaravi, M. Monleón Pradas, A. Vallés-Lluch, Scaffolds based on hyaluronan and carbon nanotubes gels. J. Biomater. Appl. 31(4) (2016) 534-543.

[33] G. Vilariño-Feltrer, C. Martínez-Ramos, A. Monleón-de-la-Fuente, A. Vallés-Lluch, D. Moratal, J.B. Albacar, M.M. Pradas, Schwann-cell cylinders grown inside hyaluronic-acid tubular scaffolds with gradient porosity, Acta Biomater. 30 (2016) 199-211.

[34] I. Ortuño-Lizarán, G. Vilariño-Feltrer, C. Martínez-Ramos, M.M. Pradas, A. Vallés-Lluch, Influence of synthesis parameters on hyaluronic acid hydrogels intended as nerve conduits. Biofabrication 8(4) (2016) 045011.

[35] C, Martínez-Ramos, L. Rodriguez Doblado, E. Lopez Mocholi, A Alastrue-Agudo, M. Sanchez Petidier, E. Giraldo, M. Monleon Pradas & V Moreno-Manzano, (2019). Biohybrids for spinal cord injury repair. *Journal of tissue engineering and regenerative medicine*, *13*(3), 509-521

[36] J. El Haskouri, J.M. Morales, D. Ortiz de Zárate, L. Fernández, J. Latorre, C. Guillem, A. Beltrán, D. Beltrán, P. Amorós, Nanoparticulated silicas with bimodal porosity: chemical control of the pore sizes, Inorg. Chem. 47(18) (2008) 8267-8277.

[37] L. Huerta, C. Guillem, J. Latorre, A. Beltrán, R. Martínez-Máñez, M.D. Marcos, D. Beltrán, P. Amorós, Bases for the synthesis of nanoparticulated silicas with bimodal hierarchical porosity, Solid State Sci. 8(8) (2006) 940-951.

[38] J. El Haskouri, D. Ortiz de Zárate, C. Guillem, J. Latorre, M. Caldés, A. Beltrán, D. Beltrán, A.B. Descalzo, G. Rodríguez-López, R. Martínez-Mañez, M.D. Marcos, P. Amorós, P. Silica-based powders and monoliths with bimodal pore systems, Chem. Commun. 4 (2002) 330-331.

[39] D. Marianiova, L. Lapčík, Electrical conductivity measurements of hyaluronic acid and collagen, Colloid Polym. Sci. 271(2) (1993) 143-147.

[40] Z. Spitalsky, D. Tasis, K. Papagelis, C. Galiotis, Carbon nanotube–polymer composites: chemistry, processing, mechanical and electrical properties, Prog. Polym. Sci. 35(3) (2010) 357-401.

[41] S.E. Moulton, M. Maugey, P. Poulin, G.G. Wallace, Liquid crystal behavior of single-walled carbon nanotubes dispersed in biological hyaluronic acid solutions, J. Am. Chem. Soc. 129(30) (2007) 9452-9457.

[42] S.M. Sze, L. Ming-Kwei, Semiconductor devices: Physics and technology, second ed., John Wiley & Sons Inc., Hoboken, 2002.

[43] G. Socrates, Infrared and Raman Characteristic Group Frequencies: Tables and Charts, third ed., John Wiley & Sons Inc., Hoboken, 2004.

[44] S. Di Cio, J.E. Gautrot, Cell sensing of physical properties at the nanoscale: Mechanisms and control of cell adhesion and phenotype, Acta Biomater. 30 (2016) 26-48.

[45] P.J. Flory, Principles of Polymer Chemistry, Cornell University, Ithaca, NY, 1953, 541-594.

[46] X. Zeng, J. Cai, J. Chen, Y. Luo, Z.B. You, E. Fotter, Y. Wang, B. Harvey, T. Miura, C. Backman, G.J. Chen, M.S. Rao, W.J. Freed, Dopaminergic differentiation of human embryonic stem cells, Stem Cells 22(6) (2004) 925-940.

[47] P. Sensharma., G. Madhumathi ,R.D. Jayant, & A.K. Jaiswal, Biomaterials and cells for neural tissue engineering: Current choices. *Materials Science and Engineering: C*, *77*, (2017) 1302-1315.

[48] E. Roussa, K. Krieglstein, GDNF promotes neuronal differentiation and dopaminergic development of mouse mesencephalic neurospheres, Neurosci. Lett. 361(1) (2004) 52-55.